Probing the Mechanism of GSH Activation in Schistosoma haematobium Glutathione-S-transferase by Site-directed Mutagenesis and X-ray Crystallography

ARTICLE *in* JOURNAL OF MOLECULAR BIOLOGY · AUGUST 2006

Impact Factor: 4.33 · DOI: 10.1016/j.jmb.2006.05.040 · Source: PubMed

doi:10.1016/j.jmb.2006.05.040 J. Mol. Biol. (2006) 360, 678–689

JMB

Available online at www.sciencedirect.com

SCIENCE DIRECT®

ELSEVIER

Probing the Mechanism of GSH Activation in *Schistosoma haematobium* Glutathione-*S*-transferase by Site-directed Mutagenesis and X-ray Crystallography

Paola Baiocco[1]†, Louise J. Gourlay[1]†, Francesco Angelucci[1] Josette Fontaine[2], Maxime Hervé[2], Adriana E. Miele[1], François Trottein[2] Maurizio Brunori[1] and Andrea Bellelli[1]*

[1]*Department of Biochemical Sciences "A. Rossi Fanelli" and Istituto Pasteur- Fondazione Cenci Bolognetti, University of Rome "La Sapienza" Rome, Italy*

[2]*Institut National de la Santé et de la recherché Médicale, Unité 547, Institut Pasteur de Lille Lille, France*

**Corresponding author*

During turnover, the catalytic tyrosine residue (Tyr10) of the sigma class *Schistosoma haematobium* wild-type glutathione-*S*-transferase is expected to switch alternately in and out of the reduced glutathione-binding site (G-site). The $Tyr^{out}10$ conformer forms a π-cation interaction with the guanidinium group of Arg21. As in other similar glutathione-*S*-transferases, the catalytic Tyr has a low pK_a of 7.2. In order to investigate the catalytic role of Tyr10, and the structural and functional roles of Arg21, we carried out structural studies on two Arg21 mutants (R21L and R21Q) and a Tyr10 mutant, Y10F. Our crystallographic data for the two Arg21 mutants indicate that only the $Tyr^{out}10$ conformation is populated, thereby excluding a role of Arg21 in the stabilisation of the out conformation. However, Arg21 was confirmed to be catalytically important and essential for the low pK_a of Tyr10. Upon comparison with structural data generated for reduced glutathione-bound and inhibitor-bound wild-type enzymes, it was observed that the orientations of Tyr10 and Arg35 are concerted and that, upon ligand binding, minor rearrangements occur within conserved residues in the active site loop. These rearrangements are coupled to quaternary rigid-body movements at the dimer interface and alterations in the localisation and structural order of the C-terminal domain.

Keywords: glutathione-*S*-transferase; schistosomiasis; π-cation interaction; mutagenesis; GSH activation

Introduction

Glutathione-*S*-transferase (GST) is an important target for the development of vaccines and drugs against schistosomiasis, the second most common parasitic disease in the world, which affects 200 million people.[1] A promising research area in the patho-physiology of schistosomiasis deals with the metabolism of eicosanoids produced by the parasite. It has been established that prostaglandin D_2 (PGD_2) blocks the host's immune response by inhibiting migration of Langerhans cells during infection, and it may be important for parasite fertility. One of the key enzymes responsible for PGD_2 synthesis in schistosomes is GST, which is endowed also with the canonical function of promoting the excretion of potentially toxic compounds by the nucleophilic addition of the tripeptide reduced glutathione (GSH). An important step in the GST catalytic cycle is the activation of GSH to GS^-.[2] In the GSTs belonging to the alpha, mu, pi and sigma classes, GSH activation results from several contributions, including a H-bond interaction with the catalytic tyrosine residue, which lowers the pK_a of the GSH. In the enzymes from other classes, the catalytic residue is either cysteine or serine.[2,3] The ionisation of GSH is important also for the prostaglandin isomerase activity of the sigma class GSH-

† P.B. and L.J.G. contributed equally to this work.

Abbreviations used: GSH, reduced glutathione; wtGST, wild-type glutathione-*S*-transferase; GTX, *S*-hexyl glutathione; Sh28GST, 28 kDa GST from *Schistosoma haematobium*; CDNB, 1-chloro-2,4-dinitrobenzene; PGD_2, prostaglandinD_2.

E-mail address of the corresponding author: andrea.bellelli@uniroma1.it

dependent PGD_2 synthase, in which GSH works as a cofactor and not as a co-substrate.[4]

GSH activation involves numerous H-bond interactions, which can be divided into two networks: a direct network (first-sphere interactions) and an indirect one (second-sphere interactions). The first sphere described here comprises direct interactions with the catalytic residue Tyr10. The second sphere involves interactions among other G site residues that generate the electrostatic environment suitable to yield GSH binding and activation.

In the crystal structure of *Schistosoma haematobium* wild-type GST[5] (wtGST), the catalytic Tyr10 is present in a double conformation: an activating conformer ($Tyr^{in}10$), with the phenoxyl group of Tyr10 projecting towards the G-site, forming a H-bond with the thiolate of GSH; and a non-activating conformer ($Tyr^{out}10$) with the phenoxyl ring projecting towards the solvent, which has not been reported before. In this novel $Tyr^{out}10$ conformer, the phenoxyl ring of Tyr10 is involved in a π-cation interaction with the guanidinium group of Arg21.[6] In a closely-related mu class GST, an on-face interaction has been observed between the catalytic Tyr6 in the G site and a threonine residue (T13), and it has been confirmed to be essential for lowering the pK_a of Tyr6.[7] Arg21 is strictly conserved in GSTs containing a catalytic tyrosine residue and kinetic studies carried out on the human alpha class GST suggest that it is important for GSH and inhibitor binding.[8]

As for other Tyr-containing GSTs, the catalytic Tyr residue in wtGST has a low pK_a of 7.2.[5] It was proposed that the two conformations of Tyr10 are both populated during catalysis. When solvent-facing, the π-cation interaction with Arg21 would lower the pK_a of Tyr10 and consequently favour deprotonation.[5] Thus, GSH may combine with either the Tyr^{out} conformer, which switches into the G site as a tyrosinate base where it extracts the GSH proton, or with the Tyr^{in} conformer, which would act as a H-bond donor. In either case, the pK_a of GSH would be lowered significantly.[5]

To test this catalytic mechanism, we designed and expressed site-directed mutants of Arg21 that lack the π-cation interaction. In these mutants, the catalytic Tyr displays a much higher $pK_a \geq 9$. In order to characterise the local and overall conformational changes that occur when Tyr10 switches between the two positions, we carried out extensive crystallographic studies on wild-type and mutant GSTs. For the first time, we were able to trap only the $Tyr^{in}10$ conformer, solving the structure of wtGST, under saturating conditions of GSH and a competitive inhibitor, *S*-hexyl glutathione (GTX). We present the crystal structure of a mutant of the catalytic Tyr (Y10F) and of two Arg21 mutants (R21L, both apo and GSH-bound, and R21Q). Analysis of the Arg21 mutants proves that the π-cation interaction is not needed to dictate the orientation of Tyr10 in the G site. However, titration experiments carried out on wild-type and mutant proteins confirm the predicted role of Arg21 in lowering the pK_a of Tyr10. The crystal data highlight a concerted, previously undetected, movement of Arg35 in relation to Tyr10 conformer position. Complementary functional studies confirm the important catalytic role of Tyr10, given that both Arg21 mutants are significantly less active than wtGST. Finally, we show that the global structure is unaffected by the mutations, but ligand binding is associated with a quaternary rigid-body movement that is reported here for the first time.

Results

Cloning, expression and purification of wild-type and mutant proteins

The successful cloning and expression of all proteins yielded approximately 20 mg to 30 mg of pure protein/500 ml culture, as judged by SDS-PAGE (results not shown).

Structural studies

There is no significant difference in the overall tertiary structures of R21L, R21Q, Y10F and wtGST. The N-terminal region of each monomer (residues 1–88) has the typical thioredoxin-like fold constituted by a four-stranded β-sheet flanked by three α-helices. The C terminus (residues 89–211) is composed of six α-helices and differs in mutant and wild-type proteins only with respect to the degree of structural constraint and location, as described below.

wtGST in complex with GSH and GTX

As we showed in our previously published structures of GSH-bound wtGST (crystallised at pH 7.4), Tyr10 is always present in a double conformation,[6] so we attempted to trap only the $Tyr^{in}10$ conformer by adjusting the crystallisation conditions. Structures of wtGST with only the $Tyr^{in}10$ conformer were obtained at low pH (6.0), in the presence of a saturating concentration of GSH or of the competitive inhibitor GTX. As the GSH-bound wtGST (pH 6.0) is highly superimposable with GTX-bound wtGST, only the latter is discussed here. The first-sphere polar interaction between the sulphur atom of GTX and the hydroxyl group of Tyr10 (3.1 Å), and the characteristic second-sphere interactions between the inhibitor backbone and the region of the polypeptide chain that forms the G-site, are conserved. As reported for the human alpha class GST,[9,10] the last nine or ten C-terminal residues were observed to interact with the N terminus, specifically at the G-site.

The structure of GTX-bound wtGST revealed that Arg35 is located in the cavity that would be occupied by $Tyr^{out}10$, forming a H-bond with Asp33 and Asn12. Comparison with published

structures reveals that the position of Arg35, which is in close proximity to the G-site, depends on the orientation of Tyr10, as shown in Figures 1 and 2.[6] The high degree of conservation of Arg35 was established by searching the entire SwissProt database, using the query motif: [Y] 7X [E,Q,H] 2X [R] 10-11X [E,D] 1-2X [R,K]. This motif was found in 65 out of 95 alpha, mu, pi and sigma class GSTs, all containing tyrosine in the catalytic site; the same motif, however, was not found in the other 83 GSTs, which contain a catalytic serine or cysteine residue. Structural analysis of all existing crystallographic data for sigma class GSTs (containing only $Tyr^{in}10$) also highlighted the presence of the interaction between Arg35 and Asp33, which, from our structure, was found to be responsible for closure of the $Tyr^{out}10$ pocket. Furthermore, the GTX-bound and GSH-bound states of wtGST have structured C-terminal regions that interact with the N terminus (Figure 3).

Y10F

The mutant Y10F was crystallised under the same growth conditions and in the same space group as wtGST.[6] One GSH molecule was bound per monomer and its occupancy was found to be approximately 80%. Functional studies (see below) demonstrate that this mutant is catalytically inactive and that it does not deprotonate the bound GSH, as expected. As for the wild-type enzyme, the N-terminal domain and the dimer interface were seen to be flexible, as indicated by the high *B*-factors for the residues belonging to these regions. Likewise, Phe10 was found in a double conformation with the π-cation interaction with Arg21 being preserved for the $Phe^{out}10$ conformer. The only noticeable difference in comparison with wtGST regards the position of Arg16 in the G-site, that was located further away than usual (3.8 Å) from the sulphur atom of GSH. It is understood that Arg16 stabilises the thiolate in alpha class GSTs;[11] such stabilisation does not occur in Y10F, as the thiolate is not formed.

R21L and R21Q

The principal differences between mutant and wild-type structures occur in the flexible N-terminal loop (residues 12–35) located in close proximity to the active site. Moreover, a portion of the N terminus of monomer B of R21L (residues 59–65, involved in the formation of the G-site) seems to be very flexible, characterised by poor electron density and a higher than average *B*-factor.

Structurally, the R21Q mutant is very similar to R21L, as revealed by the superimposition yielding an rmsd value of 0.87 Å. The principal differences concern the last five amino acid residues of R21Q (206–211), which do not appear in the electron density maps. Overall, the superimposition of monomer A is better than that of monomer B. In the latter, two loops, comprising residues 35–53 and 60–66, are slightly different.

On the basis of the observation that the π-cation interaction is present in the $Tyr^{out}10$ conformer, it was expected that mutation of Arg21 should favour the $Tyr^{in}10$ conformer. On the contrary, only the $Tyr^{out}10$ conformer was populated in these two mutants, showing that the energy contribution of the π-cation interaction is not relevant as compared with other interactions of $Tyr^{out}10$. This result allowed us to compare the structure of the enzyme with $Tyr^{out}10$ only, with

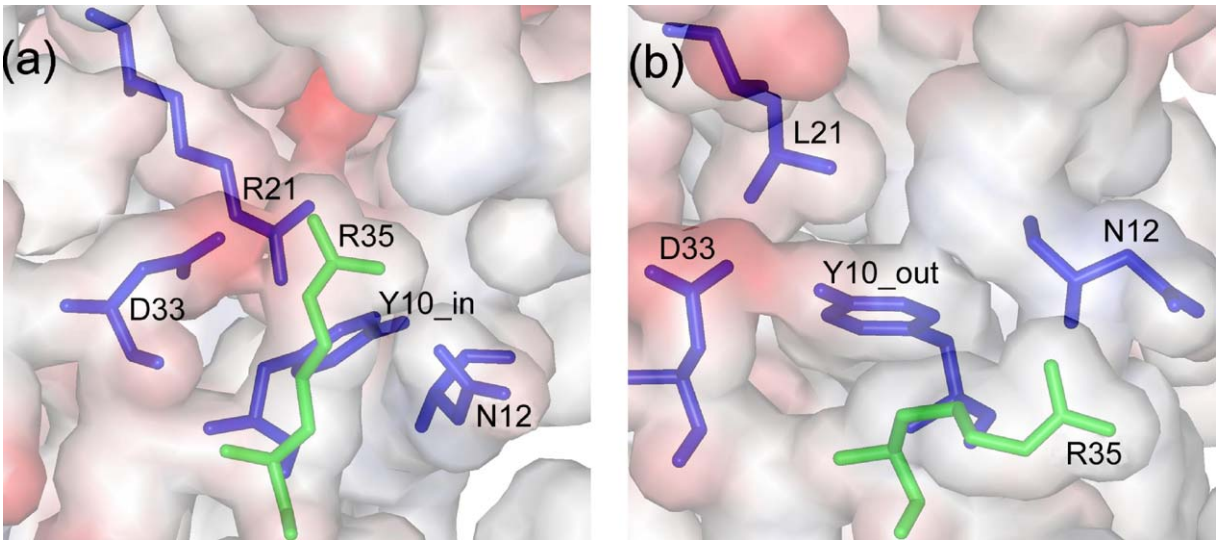

Figure 1. The movement of conserved Arg35. The two alternative positions of Arg35 were observed in the structures of (a) GTX-bound wtGST showing only the $Tyr^{in}10$ conformer and (b) R21L showing the $Tyr^{out}10$ conformer. Arg35 is indicated by green sticks, whereas other important residues are indicated by blue sticks. This Figure was generated using ViewerLite 4.2 (Accelrys Inc.).

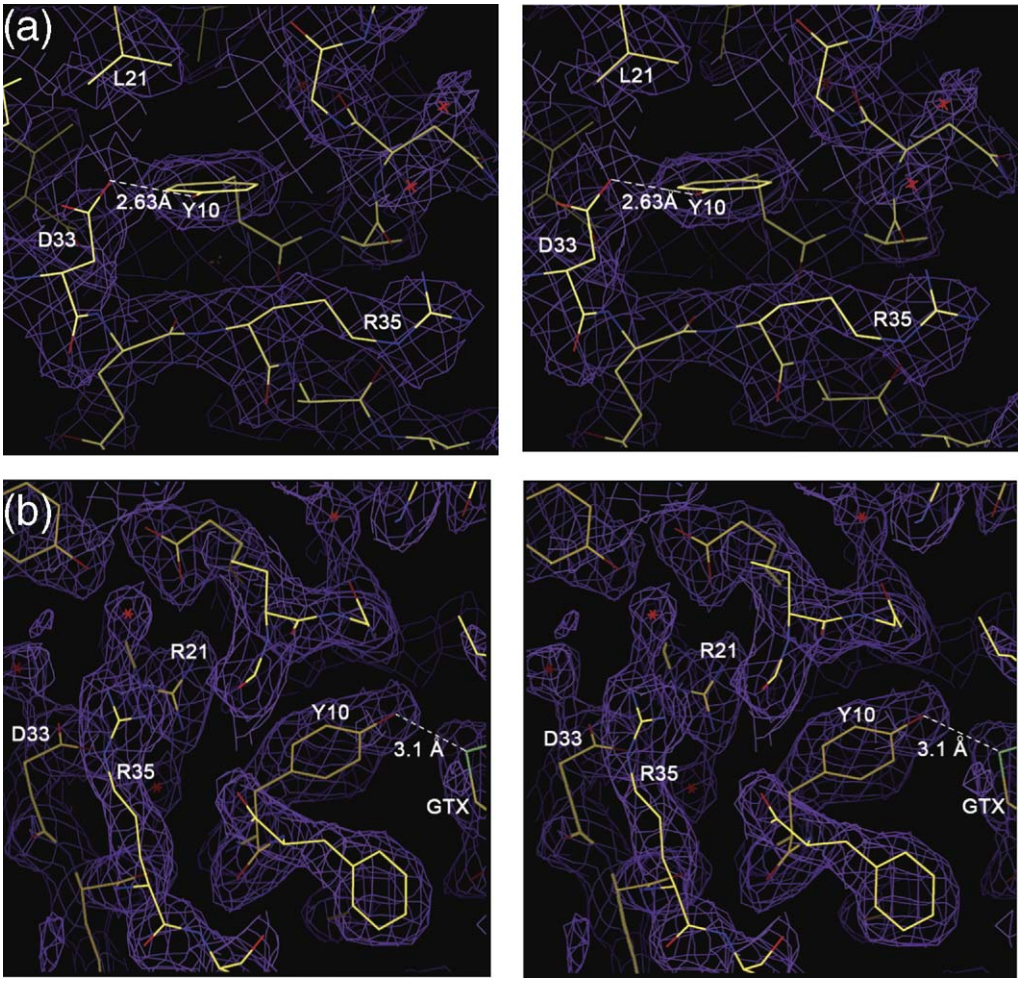

Figure 2. Stereo views of the electron density ($2F_o$–F_c at 1σ) showing the two conformers of Tyr10 in the G-site. (a) R21L, showing Tyr^{out}10 at H-bond distance from Asp33. The new residue, Leu21 is at a distance of 4 Å from Tyr10. Tyr^{out}10 hinders the movement of the Arg35 side-chain, as displayed in Figure 1(b). (b) GTX-bound wtGST, showing the polar interaction between the hydroxyl group of the Tyr^{in}10 and the sulphur atom of GTX. Tyr10, Arg21, Asp33 and Arg35 are orientated as shown in Figure 1(a).

that of the Tyr^{in}10 conformer (wtGST/GTX). This comparison highlighted some concerted movements that could not be detected in the previous structures (Figure 2).

Mutating Arg21 to Leu disrupts three important interactions formed between Arg21(NH1) and Asp33(OD1), Glu18(OE2) and Gly13(O) at distances of 3.1 Å, 2.8 Å and 2.8 Å, respectively. Mutating Arg21 to Gln also results in the loss of the above-mentioned interactions with Gly18 and Glu13; however, the H-bond between Asp33(OD1) and Gln21(OE1) is maintained (2.9 Å).

Contact comparisons were made between Tyr^{out}10 and other active site residues in GSH-bound wtGST[6] and R21L, as described in Materials and Methods. In wtGST, there is no interaction between Tyr^{out}10 and other residues at a distance less than 3 Å, except for the π-cation interaction with Arg21. In R21L, the hydroxyl group of Tyr10 forms a H-bond (2.6 Å) with Asp33(OD2), which may compensate for the loss of the π-cation interaction seen in wtGST; however, the structure of R21Q shows that Tyr^{out}10 does not interact with Asp33 (OD2). Therefore, we conclude that the π-cation bond is not the primary energetic contribution that stabilises Tyr^{out}10, consistent with the observation that this conformer makes contacts with ten other residues.[5]

Fully saturated GSH-bound R21L

The overall structure of GSH-bound R21L is less-ordered than GSH-bound wtGST in the active site and the C-terminal regions. The electron density corresponding to the last four C-terminal amino acids is absent, implying that this region is highly flexible. Tyr10 is found in a double conformation; in Tyr^{out}10, the H-bond between its hydroxyl group and Asp33(OD2) (2.6 Å) is observed once more. Tyr^{in}10 interacts with GSH in the G-site through interactions similar to those for the wild-type, and the only significant difference is the distance between Tyr10(OH) and GSH(S), which is slightly longer (3.9 Å) than in the wild-type, and a few additional interactions between the guanidinium group of Arg16 and GSH.

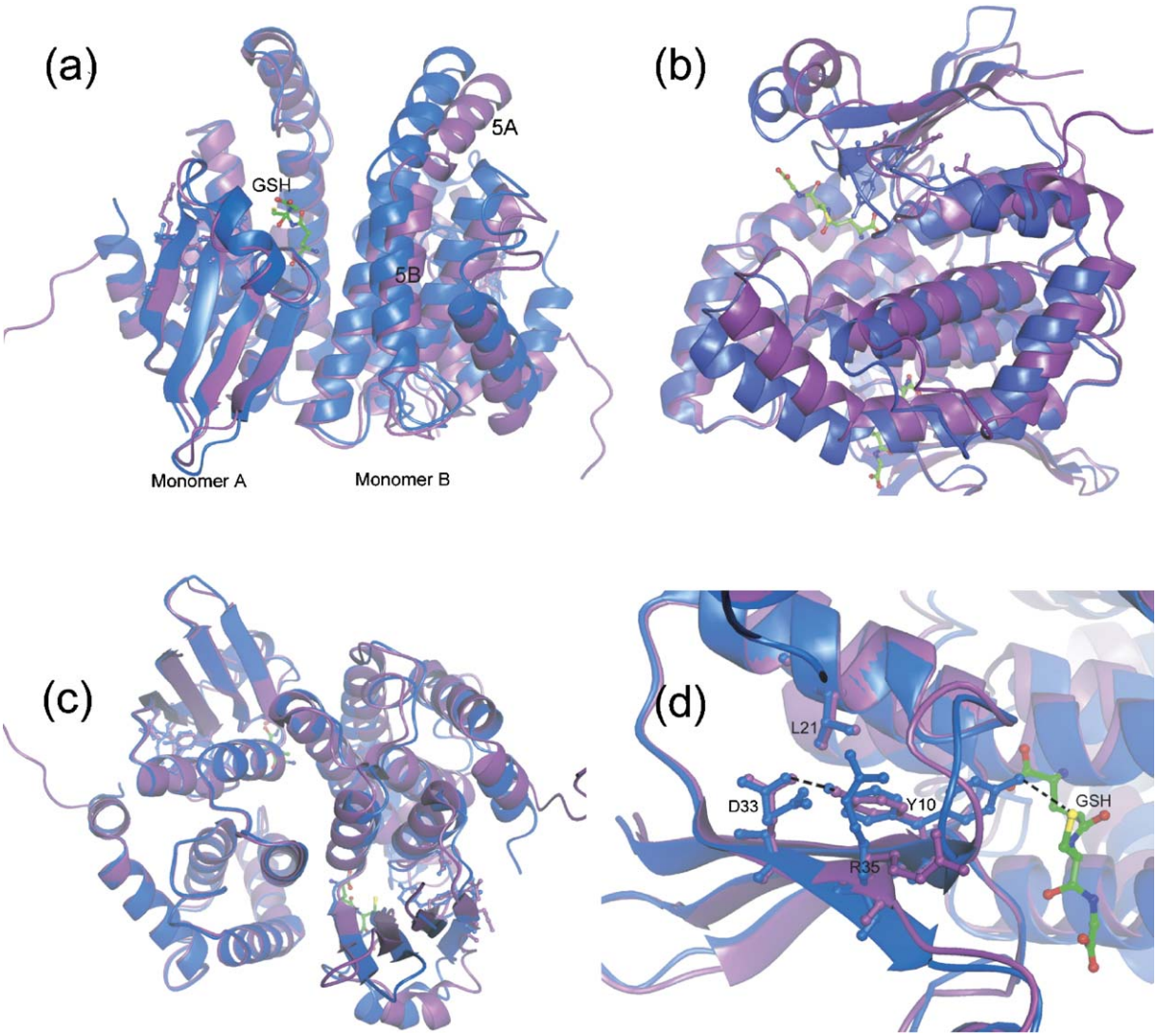

Figure 3. Overall quaternary structural changes upon ligand binding. Superimposition of structures was made using the Coot program,[32] fixing monomer A in order to visualise the movements in helices 5A and 5B in monomer B. Analogous superimpositions were made to follow monomer A movements (not shown). (a) Superimposition of R21L (purple) and GSH-bound R21L (blue). (b) Side-view of helix movement in monomer B. (c) Bottom, cross-sectional view of R21L and GSH-bound R21L. (d) The active site of R21L and GSH-bound R21L.

Structural comparison of wtGST and the arginine mutants: local effects

In order to understand the conformational changes occurring in the Tyr^{out} pocket, we compared two extreme cases: GTX-bound wtGST (exclusively Tyr^{in}10) and unbound R21L (exclusively Tyr^{out}10), using the Cast-P program‡, which is used to estimate various parameters relating to the size and volume of solvent-accessible cavities and pockets present in proteins and other molecules (Table 1).

Key observations were made related to the position of one active site loop residue, Arg35. In GTX-bound wtGST, Arg35 interacts with Asp33 and Asn12; however, in R21L such interactions are lost because Arg35 leaves this cavity, fully occupied by the Tyr^{out}10 conformer (Figure 1). In GTX-bound GST, the pocket is closed to the solvent (no mouth openings) and has a molecular surface area of 41 Å^2; in R21L the pocket contains one mouth opening and has a larger molecular surface area (169 Å^2). Therefore, it can be seen that the catalytic mechanism and flipping of the tyrosine is coupled to a change in molecular surface area and solvent accessibility of the Tyr^{out}10 pocket. These changes depend on a concerted rearrangement of the amino acid residues that form this pocket. Analysis of the *B*-factors for amino acids in the pocket indicates that several key residues exhibit high mobility. The *B*-factor for the side-chain of Arg35 is slightly higher (46 Å^2) than the average *B*-factor for the side-chains of the entire protein (41 Å^2) in

‡ http://cast.engr.uic.edu/cast/

Table 1. Volume and internal surface area estimates made for the Tyr^{out}10 cavity

Molecule	No. mth[a]	Area ms[b] (Å^2)	Vol ms[c] (Å^3)
wtGST	1	100	86
wtGST+GTX	0	74	41
R21L	1	169	153
R21L+GSH	2	280	255
R21Q	2	199	281

Estimates were made for GTX-bound wtGST, R21L, GSH-bound R21L and R21Q using the Cast-P program and a probe radius of 1.0 Å.[33] For R21L and R21Q, pockets were selected substituting Tyr^{out}10 with an alanine residue with the same C^{α} and C^{β} coordinates. For GTX-bound wtGST and GSH-bound R21L, pockets were selected according to the presence of Arg21(NH2) and the C^{α} and C^{β} atoms of Tyr10.

[a] No._mth is the number of mouth openings for each pocket.

[b] Area ms is the molecular surface area of the cavity.

[c] Vol ms is the volume enclosed in the molecular surface area of the cavity.

wtGST, while in GTX-bound wtGST it is the same (20 Å^2) as the average for the protein (21 Å^2).

Global (quaternary) effects

So far we have considered the local effects of ligand binding and the mutations. However, we considered also the global effects on the quaternary structure of the dimer. In GSTs, dimerisation is highly specific, class-dependent and believed to be essential for full catalytic activity. The two monomers of the sigma class enzymes interact *via* polar interactions, mainly through helix 5 from each monomer.[12] In Sh28GST, Asp104 is important and participates in interfacial interactions *via* ionic bonds with GSH.[6] We observed, however, that in GTX-bound wtGST, Asp104 does not participate in any interfacial interaction. With regards to the Arg mutants, there is a minor rearrangement of interactions at the dimer interface, and both R21L and R21Q were confirmed to be dimers by sedimentation equilibrium ultracentrifugation (results not shown).

With regards to the global structure, superimposition of R21L in the presence or in the absence of GSH revealed a hitherto undetected quaternary rearrangement regarding helix 5A (residues 118–129) and helix 5B (residues 132–145) at the dimer interface (Figure 3(a) to (d)). Upon ligand binding, helices 5A and 5B of each monomer rigidly move towards each other, closing the V-shaped fork present at the dimer interface by about 14°, corresponding to a maximum shift of 6 Å at the top of helix 5A. Superimposition of ligand-bound wtGST and Y10F also illustrated this movement, confirming that it is not a consequence of the Arg21 mutation. Closure of the V-shape upon binding of GSH is coupled to movement of the last five C-terminal residues, from an unstructured and delocalised state to a more ordered state, relocating towards the N terminus (Figure 3(a)).

Functional studies

The effect of Arg21 on the pK_a of Tyr10 and bound GSH

As previously reported, the proposed role of Arg21 is to lower the pK_a of Tyr10 by the π-cation interaction.[5] As described in Materials and Methods, titrations were carried out to determine the pK_a of Tyr10 in mutants R21L and R21Q, to be compared with the previously reported estimate for wtGST.[5] Overall, wtGST contains nine tyrosine residues per monomer. Comparison of the pH titration of wtGST with that of the mutant Y10F allowed us to assign the optically detectable transition near neutrality (pK_a=7.2) to Tyr10. As anticipated, titration of R21L and R21Q shows that the pK_a of Tyr10 is in the usual range (i.e. ~9.5), and fully supports our conclusion that the catalytically competent and conserved Tyr10 has a pK_a of 7.2, due to the π-cation interaction, which is obviously lacking in these two mutants (Figure 4). The pK_a of enzyme-bound GSH can also be determined spectroscopically, following the absorbance increase at 240 nm. We found that in the wild-type enzyme, the pK_a of bound GSH is 7.2, whereas in Y10F and the Arg21 mutants it is elevated to ≥8.5.

GSH and GTX binding experiments

The affinity of all GST variants for GSH was measured by tracing the change in tryptophan fluorescence emission with increasing concentration of GSH under equilibrium conditions. The K_d values for the arginine mutants and Y10F in comparison with that for the wtGST are summarised in Table 2. R21Q has a binding affinity for GSH comparable to that of wild-type; in contrast, the K_d of R21L indicates a tenfold lower affinity for GSH. Therefore, substitution of Arg21 with Leu influences GSH binding to a greater extent than substitution with

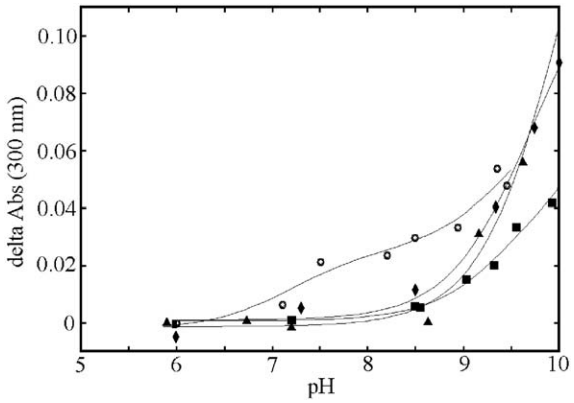

Figure 4. Tyr10 pK_a determination in wild-type and mutant proteins. Spectroscopic acid–base titrations of wild-type GST (circles), R21L (triangles), R21Q (diamonds) and Y10F (squares), carried out as described in Materials and Methods. Differential absorbance at 300 nm, shown as a function of pH. Wild-type and Y10F data are those reported previously.[5]

Table 2. Summary of steady-state and GSH/GTX binding results

Protein	k_{cat} (s^{-1})	Fluorimetry K_d (GSH) (μM)	Fluorimetry K_d (GTX) (μM)	Rapid mixing K_d (GSH) (μM)
wtGST	48	22	4.7	50
R21L	4	285	10.7	250
R21Q	0.4	21	16	
Y10F	0	21		

The k_{cat} values were calculated using the CDNB assay, as described in Materials and Methods. Dissociation constants (K_d) were calculated either by static fluorimetry or rapid mixing experiments. Values were calculated from duplicate or triplicate experiments differing by ±10%.

Gln. Similar experiments were carried out for Y10F, demonstrating that substitution of Tyr10 does not affect GSH-binding.

The binding affinity of GTX for wtGST, R21L and R21Q was measured. The K_d values indicate that the arginine mutants have binding affinities that are approx. twofold lower than that of the wild-type enzyme (Table 2). In all cases, the affinity for GTX is higher than that for GSH. In summary, the most obvious difference was seen for R21L, which has a 28-fold higher affinity for GTX than for GSH.

Steady-state and transient kinetics

Steady state kinetic measurements showed that the Tyr and both the Arg mutants had lower k_{cat} values in comparison with wtGST (Table 2). Y10F has a catalytic activity ≤1% of the total wild-type activity, confirming the fundamental catalytic role of Tyr10.

Rapid mixing experiments were carried out by measuring the decrease in fluorescence upon GSH binding, to ascertain if the velocity of this process is affected by the Arg21 mutation. Reactions for wtGST and R21L were fitted to a single or double exponential, depending on the trace (Materials and Methods). Due to the low affinity of R21L, higher concentrations of GSH were required in comparison with the wild-type (Materials and Methods). For both proteins, the K_d values obtained for GSH binding were in agreement with those calculated from equilibrium experiments, with the binding affinity of R21L for GSH being approximately fivefold weaker than that for wtGST (Table 2).

The role of wtGST and R21L in inducing GSH deprotonation was assessed in similar kinetic experiments, following the absorbance increase at 240 nm. The kinetics of binding, observed by fluorescence, was seen to be faster than that observed by absorbance, suggesting that the initially formed complex undergoes a structural rearrangement before GSH deprotonation. The K_d values estimated from fluorescence and absorbance are equal (i.e. $K_d = 50$ μM). There was no absorbance signal for R21L, a demonstration that this mutant does not significantly deprotonate GSH under our experimental conditions. This finding is fully consistent with the low catalytic activity, and supports the essential role of Arg21 in promoting the deprotonation of $Tyr^{out}10$ by lowering its pK_a.

Discussion

In the previously reported structure of *S. haematobium* GST in complex with GSH at pH 8.0, the catalytic Tyr10 exists in a double conformation.[6] Only the $Tyr^{in}10$ conformer is catalytically competent, being located at a short distance from GSH; however, the role of the $Tyr^{out}10$ conformer was presumed to be important because a π-cation interaction with the conserved Arg21 residue could lower the average pK_a of Tyr10 to approximately 7.2.[5] The resulting tyrosinate may then return to the G site for subsequent cycles of GSH activation and binding. The lower than usual pK_a of the catalytic residue is a common feature of Tyr-containing GSTs.[9–13] We describe the structural and functional studies carried out to prove this mechanism of GSH activation. Investigations were carried out, on the basis of the crystal structures of GSH-bound and GTX-bound wtGST, two arginine mutants (R21L and R21Q) and one catalytically inactive mutant (Y10F). We reveal the local changes that occur in the interactions that govern GSH activation with substitution of Tyr10 or Arg21. Furthermore, we report a novel quaternary conformational change, involving dimer organisation that occurs upon ligand or inhibitor binding.

Conformer position and structural role of Arg21

We successfully trapped the single $Tyr^{in}10$ conformation, as illustrated in the crystal structures of wtGST crystallised with GSH or GTX, and the single $Tyr^{out}10$ conformation in the structure of GSH-free Arg 21 mutants; these allowed us to compare the structural changes associated with the movements of the catalytic Tyr in wtGST. The main focus of our investigations was to elucidate the role of the π-cation interaction of Arg21 in determining the position of Tyr10 and in GSH activation.[5] It was initially proposed that substitution of Arg21, and hence removal of the π-cation interaction, would preferentially stabilise only the $Tyr^{in}10$ conformer; on the contrary, the structure of ligand-free R21L and R21Q showed that only the $Tyr^{out}10$ conformer was populated, implying that the π-cation interaction has little effect, if any, on the position of Tyr10 in the G-site. Tyr10 is once again seen in a double conformation in GSH-bound R21L, confirming that the Arg21 mutation does not prevent ligand binding.

Functional role of Arg21

Although structural data reveal that Arg21 is not required to stabilise the $Tyr^{out}10$ conformer, we proved that it is crucial to lower its pK_a. In fact, the arginine mutants bind GSH and GTX, and populate both Tyr10 conformers (in GSH-bound R21L), with the usual $pK_a \geq 9.5$. The catalytic Tyr in GSTs plays

at least two roles, i.e. it participates to activate GSH and is involved in the C-terminal rearrangement that accompanies product release.[9] We may thus enquire how the acidic nature of Tyr facilitates its functions, given that this feature is common but not ubiquitous. As suggested for several GSTs, the activation[8] of GSH is mediated by H-bonding to the catalytic Tyr,[4–13] whose low pK_a would help the complex to release one proton, while sharing the other. Whether Tyr acts as a base or an H-bond donor is discussed elsewhere,[5] but at least in some GSTs, the pK_a of Tyr is relevant to this process; this applies also to wtGST from *S. haematobium*, since we found that Y10F and the Arg21 mutants lower the pK_a of bound GSH to a significantly smaller extent than the wild-type. This finding is in agreement with other studies carried out on tyrosine-containing GSTs (i.e. GST P1-1,[14] GST M1-1[7] and rat GSTA3-3[15]), but contrasts with results obtained for the wild-type and tyrosine mutants of the human isoforms GST A1-1[16] and GSTA3-3[17] (Table 3). It seems safe to conclude that the activation of GSH is due to interaction with several residues of the active site, of which Tyr is only one, and varies in importance in different GSTs.

We may next ask how far the role of the two conformers of Tyr10 seen in wtGST can be generalised to other GSTs. As discussed by Angelucci *et al.*,[5] we suggest that at least two conditions must be met for our hypothesis to be considered for any given GST; namely (i) the p*K*a of the catalytic Tyr should be significantly lower than usual, and (ii) an external pocket is present and hosts an Arg residue approximately 11 residues away from Tyr, with its interaction network. These conditions are met by all the GSTs given in Table 3, except rat GST M1-1.

The finding that R21L is slightly more active than R21Q may be due to the H-bond between Tyr10 and Asp33, since aspartate and glutamate residues have been shown to participate as proton shuttles in several catalytic mechanisms.[18,19] Therefore, in R21L but not in R21Q, Asp33 could act as a proton acceptor and partially deprotonate Tyr10. This interpretation is in agreement with the observed increase in catalytic activity of R21L at higher pH (data not shown). Overall, these results confirm the hypothesis that the π-cation interaction between Arg21 and the Tyr^{out}10 conformer is the major determinant of the low pK_a of the catalytic residue in wtGST.[5]

Table 3. Overview of the correlation between the pK_a of bound GSH and that of the catalytic residue in tyrosine-containing GSTs2

GST isoform	pK_a of bound GSH		pK_a	References
	WT	YnF	Tyr_{cat}	
GST P1-1 (human)[14]	6.3	8.7	≥7.3	[34]
GST M1-1 (rat)[7]	6.2–6.7	7.8–8.3	10.2	[7]
GST A1-1 (human)	6.7	7.2	8.1	[9,16]
GST A3-3 (rat)	6.2±0.1	7.8±0.3	–	[15]
GST A3-3 (human)	6.1±0.1	6.5±0.2	7.9	[17]
Sh28GST	7.2	≥8.5	7.2	[5], This study

The pK_a values for bound GSH in wild-type (WT) and YnF mutant of various GSTs are listed together with the pK_a values for the catalytic tyrosine residue.

GSH and GTX binding

It has been reported for the human class alpha GST that mutation of R20A (equivalent to Arg21 in our structure) results in a reduced binding affinity for GSH and a significant loss of catalytic activity.[8] However, our GSH binding experiments demonstrate that, in the case of R21Q, the affinity is similar to that of the wild-type enzyme, whereas R21L binds GSH with a tenfold lower affinity. Although Arg21 does not participate directly in GSH binding, it forms an important direct interaction with Tyr10, and its effect on the affinity for GSH is indirect. In wtGST, the T-shaped geometry of Arg21, necessary for the π-cation interaction is held *via* H-bonds with Glu18 and Asp33. Although both Arg21 mutants lack the π-cation interaction, R21Q, but not R21L, retains the H-bond with Asp33. The conservation of this bond, together with the generally more polar properties of Gln, may account for the similar affinities observed for wtGST and R21Q. To strengthen the importance of first-sphere interactions in GSH binding, we observed that Y10F, although catalytically inactive, binds GSH with an affinity similar to that of the wild-type enzyme.

As for wtGST, there are differences in the binding interactions of GSH and GTX with R21L, which are in agreement with experiments carried out for other GST classes.[20] This higher affinity may depend on the fact that GTX ''blocks'' the Tyr^{in}10 conformer and occupies both the G-site and the H-site with its hexyl group.

Local interaction effects

A detailed analysis of the 3D structures of the three mutants, in comparison with the wild-type enzyme, shows, as expected, that the overall fold is conserved. The only significant structural differences, further to the above-mentioned Tyr10 conformer position, were confined to the G site and to the location of the C terminus with respect to the N terminus. In particular, comparison of our wtGST and Arg21 mutant structures highlighted a concerted movement of Tyr10 and Arg35. The latter residue functions as a ''gate'' to the G site, preventing or permitting entry to this pocket when Tyr^{in}10 or Tyr^{out}10 is populated, respectively. For Tyr^{out}10, the active site loop residues 9–15 are stabilised by Asn12 and Gly15. In this context, we analysed the four structures of the three mutants. Y10F (a first-sphere Tyr^{in}10 mutant) displays a G site similar to that of the wtGST; unbound R21L and R21Q (first-sphere Tyr^{out}10 mutants) show a different conformation of the active site loop, strictly related to the mutations, which lose the π-cation interaction and other contacts (see Results); GSH-bound R21L, in contrast, has a G site similar to wtGST, although the active site loop is more mobile.

Regarding the C terminus of the proteins, it can be seen clearly that ligand binding to wtGST results in a more structured C terminus, which is stabilised by contacts with the N-terminal active site loop. In contrast, in both unbound arginine mutants, the C terminus is flexible, unstructured and ''lost'' in the solvent. Such alterations in the location of the C terminus with respect to the N-terminal loop region may account for the observed relationship between the ionisation of the catalytic tyrosine and C terminus location, already seen for the human alpha class GST.[9]

Global effects

As the active site region of GSTs has been suggested to participate in the assembly of the two monomers in the dimer,[21] the global effects of ligand binding and Arg21 substitution on dimerisation and overall quaternary structure were investigated. The interfacial interactions of both R21L and R21Q were compared with inter-subunit contacts present in GTX-bound wtGST. The Arg21 mutants are still dimers, proving that Arg21 has only local effects. Interesting changes were observed at the dimer interface upon ligand or inhibitor binding to both wild-type and mutant proteins. The GST monomers interact *via* the connected helices 5A and 5B to form a V-motif that is open in the ligand-free state and closed in the bound state. Ligand-induced flexibility has been observed in various GSTs[22,23] by means of fluorescence, NMR and hydrogen-deuterium exchange mass spectroscopy; the structural changes were attributed mainly to the active site loop (so-called α-helix 2 in pi and mu classes). These studies suggest that two conformations of GSTs M1-1 and P1-1 may be present in solution, and their interconversion may be coupled to catalytically relevant structural rearrangements of the enzyme–substrate complex. Our crystallographic data agree with these findings and, in addition, highlight an overall quaternary movement involving the rigid body motion of helices 5A and 5B. These rearrangements are concerted with the movement of the C-terminal chains that become more structured and relocate next to the active site in the N-terminal domain. (Figure 3). This is in agreement with findings reporting the involvement of helix α9 of the C terminus of GST A1-1.[24] All together, our findings raise the question of whether the quaternary conformational change occurring upon GSH binding is significant to positive cooperativity.[25]

To summarise, our structural data demonstrate that Arg21 does not determine Tyr10 conformer position, and the first-sphere interaction between the GSH thiolate and the hydroxyl group of Tyr10 is conserved (as seen in GSH-bound R21L). However, minor localised interaction changes were observed with respect to Arg21 and to the position of Arg35 in the G site. Furthermore, we confirm that these mutations do not affect the global structure of the protein; and we highlight an overall quaternary change that has not been reported before and it is coupled to ligand binding. Our complementary functional studies confirm the catalytic roles of both Tyr10 and Arg21 in GSH binding and activation. Given the conservation of Arg21, Asp33, Arg35 and Tyr10, we propose that the role and the concerted movements of such residues during ligand binding may be conserved in other GSTs, and may be of more extended validity.

Materials and Methods

Cloning, expression and purification of wild-type and mutant proteins

The wtGST gene was amplified by PCR using KOD HotStart DNA polymerase (Novagen, EMD Biosciences, Darmstadt, Germany) using wtGST held in the pCR-3.1 vector as the template for the reaction, and sub-cloned into the bacterial expression vector pET-23b (Novagen). The specific forward and reverse primers used, were designed according to standard primer protocols. All reactions were carried out in a PTC-150 Minicycler™ (MJ Research Inc.). Site-directed mutagenesis of wtGST/pET-23d using specific primers was carried out using the QuikChange Site-directed Mutagenesis kit (Stratagene), according to the manufacturer's instructions. All amplified products were checked by sequencing.

Escherichia coli BL21 (DE3) pLysS bacterial cells (Novagen, Darmstadt, Germany) were transformed with the recombinant plasmids and grown at 37 °C in Luria broth, supplemented with 50 μg/ml of ampicillin. Protein expression was induced upon addition of IPTG (Sigma-Aldrich Co.) to 0.2 mM, and incubation for a further 5 h. Bacterial cells were harvested by centrifugation and the pellet (wtGST and R21L) resuspended in 30 ml of phosphate-buffered saline (PBS), pH 7.4 containing 10 mM β-mercaptoethanol (β-ME). Following sonication and centrifugation, the clarified supernatant was passed through a 5 ml GSTrap™ HP column (GE Healthcare, Uppsala, Sweden). GSH-bound wtGST and R21L proteins were eluted with 50 mM Tris–HCl (pH 7.3), 0.1 M NaCl, 10 mM GSH. Peak fractions were dialysed into PBS (pH 7.4) containing 10 mM β-ME, before concentration by ultrafiltration. Preparation of Y10F was carried out as described for wtGST.[6]

The R21Q bacterial pellet was resuspended in 20 mM Tris–HCl (pH 8.3) and the protein purified on a Sepharose 15Q ion-exchange column (GE Healthcare). Bound protein was eluted with a salt gradient (0–0.5 M NaCl) and subsequently dialysed and concentrated as described above.

GTX-bound wtGST was prepared using the purification procedure described above but eluting with 20 mM GTX instead of GSH. To obtain GSH-free proteins, wtGST and R21L were eluted with 20 mM glycine in PBS (pH 10).

All protein concentrations were determined spectroscopically, measuring the A_{280} and using an extinction coefficient of 0.96 mg/ml.

Crystallisation

All crystals were grown at 21 °C by the hanging-drop, vapour-diffusion method. When required, microseeding techniques were used to increase crystal size. Y10F was crystallised under the growth conditions reported for wtGST.[6] R21L crystallised in a drop containing a 1:1 (v/v) ratio of protein (15 mg/ml) to well solution (PBS (pH 7.4), 2.3 M ammonium sulphate, 5 mM β-ME, 10% (w/v) PEG 200). R21Q (10 mg/ml) crystals grew in a well solution of 0.2 M MES (pH 6.0), 2.5 M ammonium sulphate, 5 mM β-ME. Crystals of wtGST complexed with GTX grew in a well solution of 0.2 M MES (pH 6.0), 20% (w/v) PEG 3350, 5 mM β-ME. Crystals of GSH-bound wtGST were grown at pH 6.0 at a 1:1 (v/v) ratio of protein (15 mg/ml in PBS (pH 7.4), 5 mM β-ME, 10 mM GSH) to well solution of 0.2 M imidazole/malate buffer (pH 6.0), 10% (w/v) PEG 4000. Crystals of GSH-bound R21L grew in a 1:1 (v/v) ratio of protein (10 mg/ml) in PBS (pH 7.4), 5 mM β-ME, 10 mM GSH to a well solution of 0.1 M sodium acetate (pH 5.5), 25 % (w/v) PEG 5000 MME.

All crystals were cryo-cooled in well solution containing a final glycerol concentration of 18% (w/v).

Data collection and processing

Diffraction data were collected at resolutions ranging from 2.0 Å to 2.5 Å at ELETTRA (Trieste, Italy), ESRF (Grenoble, France) and DESY (Hamburg, Germany). Space groups were determined by autoindexing and processed using the HKLsuite.[26] The statistics of crystallographic data collection and model refinement are shown in Table 4.

Molecular replacement, model building, and refinement

The 3D structures were solved by molecular replacement,[27,28] using the structure of wtGST as a model (PDB entry *1OE7*).[6] All structures were refined using REFMAC5[29] and fit to generated electron density maps using Xtalview/Xfit.[30,31] All data were refined to give satisfactory final *R*-factors (Table 4).

Quality of the structural data

The electron density for the final models of R21L and wtGST in complex with GTX or GSH is well defined for residues 4–211 in both chains A and B. The electron density for the models of R21Q, GSH-bound R21L and Y10F, instead, is not well defined in the C-terminal region and lacks residues 207–211 in the monomeric chain A. All structures display good geometry and no residue is present in the disallowed region of the Ramachandran plot (Table 4).

Steady state determinations

The catalytic activity was determined spectroscopically using an HP845x UV-visible spectrophotometer (Hewlett-Packard) under steady-state conditions, using the chromogenic substrate 1-chloro-2,4-dinitrobenzene (CDNB; Sigma-Aldrich). Experiments were carried out measuring the absorbance increase at 340 nm at 20 °C over 120 s. The assay was initiated upon addition of the enzyme to a 1 ml

Table 4. Summary of crystallographic data

	Protein					
	R21L	R21L+GSH	R21Q	Y10F+GSH	wtGST+GTX	wtGST+GSH
Crystallisation conditions	2.3 M AS 10% PEG 200 PBS (pH7.4) 5 mM β-ME	25% PEG 5000 MME 0.1 M sodium acetate (pH 5.5)	2.5 M AS 0.2 M Mes (pH 6.0) 5 mM β-ME	2.4 M AS 0.1 M Tris (pH 7.4) 5 mM β-ME	20% PEG 3350, 0.2 M Mes (pH 6.0) 5 mM β-ME	10% PEG 4000 0.2 M imidazole/ malate (pH 6.0)
A. *Data collection statistics*						
Space group	*I*23	$P322_1$	$P2_1$	$P2_1$	$P3_2$	$P322_1$
Unit cell dimensions						
a (Å)	148.8	53.2	53.5	53.2	52.8	53.3
b (Å)	148.8	53.2	77.5	77.6	52.8	53.3
c (Å)	148.8	141.8	53.5	53.1	141.4	142.4
β (deg.)			94.3	94.26		
No. unique reflections	24,373	15,440	29,520	23,175	18,295	8261
I/σ	10.2	19.9	14.9	35.8	11.3	10.2
Completeness (%)	99.8	99.35	91.6	96.64	99.0	99.11
Average redundancy	22.0	5.6	4.6	4.1	3.5	8.3
R_{merge}	0.063	0.055	0.053	0.065	0.122	0.070
B. *Refinement statistics*						
Resolution	30–2.26	20–2.0	30–2.0	50–2.1	30–2.2	20–2.49
R-factor	0.206	0.189	0.219	0.221	0.178	0.194
R_{free} [a]	0.270	0.239	0.292	0.288	0.243	0.252
rmsd from ideal						
Bond lengths (Å)	0.013	0.009	0.012	0.011	0.011	0.013
Bond angles (deg.)	1.875	1.208	1.3	1.245	1.432	1.483
No. molecules/a.u.	2	1	2	2	2	1
Ramachandran plot						
Most favoured regions (%)	99.5	100	99.3	99.5	99.7	100
Generously allowed regions (%)	0.5	0	0.7	0.5	0.3	0
Disallowed regions (%)	0	0	0	0	0	0

[a] R_{free} was calculated from 5% of reflections taken from the raw data.

quartz cuvette containing GSH and CDNB in 0.1 M potassium phosphate (pH 7.0). Experiments were carried out at constant concentrations (2 mM) of GSH and CDNB. The wild-type and R21L protein concentrations used were 0.1 μM and 2.4 μM, respectively. Data were fitted using Origin 7 Server Software (Northampton, MA, USA). Similar experiments were carried out for GTX at a constant concentration (2 mM) of CDNB and various concentrations of GSH.

Fluorescence measurements

Intrinsic fluorescence quenching was followed at 20 °C, upon ligand addition, using a Spex Fluoromax spectrofluorimeter (excitation wavelength 280 nm, emission range 300–400 nm). Protein (1 μM) was added to a 2 ml cuvette containing 0.1 M potassium phosphate (pH 7.0). Similar experiments were carried out for GTX using protein concentrations of 1 μM and 0.5 μM for wtGST and R21L, respectively. All experimental data were analysed using MATLAB 5.3.

Stopped-flow experiments

Rapid mixing experiments were carried out at 20 °C using an Applied PhotoPhysics stopped-flow apparatus (instrument dead-time ~2 ms). GSH binding was measured, following the tryptophan fluorescence decrease (excitation wavelength 280 nm, 320 nm cut-off filter, 1 nm slit). Equal volumes of protein and GSH were mixed to give a final concentration of 5 μM wtGST and 10 μM R21L and a range of concentrations (15–50 μM) of GSH. The wtGST experiments were carried out in 0.1 M potassium phosphate buffer (pH 7.0), whereas R21L experiments were carried out in the same buffer at pH 8.0. Reactions were recorded over 0.2 s. Averages of multiple traces collected for each concentration of GSH were fitted to a single exponential using an Applied PhotoPhysics Spectrakinetic Workstation version 4.46 and were used to determine the k_{off} of GSH for the protein.

The ability of wtGST and R21L to deprotonate GSH was also assessed by rapid mixing experiments, under the above conditions, following the absorbance increase at 240 nm at different concentrations (15–50 μM for wtGST and 125–500 μM for R21L) of GSH.

Determination of the pK_a of Tyr10 and bound GSH

The ionisation of the nine tyrosine residues was detected spectrophotometrically using an HP845x spectrophotometer (Hewlett-Packard), measuring the concentration of tyrosinate from the intrinsic absorbance at 293 nm ($\Delta\varepsilon$ of 2400 M^{-1} cm^1) as a function of pH. Mixtures of 50 mM sodium borate and 50 mM sodium phosphate were prepared to cover a pH range from 6.0 to 10. Difference spectra at each pH were recorded by reference to the protein at pH 6.0. The ionisation of bound GSH was determined using a similar experimental procedure, and taking advantage of the absorbance change at 240 nm. The concentrations of R21L and R21Q ranged from 15 μM to 35 μM.

Data Bank accession codes

All the structures have been deposited in the PDB with the entries 2C80 (GTX-bound wtGST), 2CA8 (GSH-bound wtGST pH 6), 2F8F (GSH-bound Y10F), 2C8U (R21Q), 2CAI (R21L) and 2CAQ (GSH-bound R21L).

Acknowledgements

This project was supported by Progetto di Ateneo (University of Rome ''La Sapienza''), Consorzio Interuniversitario Biotecnologie (Urbino, Italy) and the MIUR, FIRB 2003 ''Biologia strutturale post-genomica: sviluppo di infrastrutture per la cristallografia delle proteine''. P.B. is supported by Elettra (Trieste, Italy). We are grateful for the ELETTRA (Trieste, Italy), DESY (Hamburg, Germany) and ESRF (Grenoble, France) synchrotron radiation facilities. The European Community - Research Infrastructure Action under the FP6 Structuring the European Research Area Programme contract number: RII3-CT-2004-506008 is gratefully acknowledged for travel and accommodation support. We thank the Bio Molecular Research Sequencing Service (University of Padova, Italy). We also thank Dr Laura Giangiacomo who carried out the ultracentrifugation experiments.

References

1. WHO Expert Committee on the Control of Schistosomiasis. (1993). *The Control of Schistosomiasis*, *WHO Technical Report Series no. 830*, WHO, Geneva.
2. Armstrong, R. N. (1997). Structure, catalytic mechanism, and evolution of the glutathione S-transferase. *Chem. Res. Toxicol.* **10**, 2–18.
3. Sheehan, D., Meade, G., Foley, V. M. & Dowd, C. A. (2001). Structure, function and evolution of glutathione transferases: implications for classification of non-mammalian members of an ancient enzyme superfamily. *Biochem. J.* **360**, 1–16.
4. Kanaoka, Y., Ago, H., Inagaki, E., Nanayama, T., Miyano, M., Kikuno, R. *et al.* (1997). Cloning and crystal structure of hematopoietic prostaglandin D synthase. *Cell*, **90**, 1085–1095.
5. Angelucci, F., Baiocco, P., Brunori, M., Gourlay, L., Morea, V. & Bellelli, A. (2005). Insights into the catalytic mechanism of glutathione S-transferase: the lesson from *Schistosoma Haematobium*. *Structure*, **13**, 1241–1246.
6. Johnson, K. A., Angelucci, F., Bellelli, A., Hervé, M., Fontaine, J., Tsernoglou, D. *et al.* (2003). Crystal structure of the 28(kDa glutathione S-transferase from Schistosoma haematobium. *Biochemistry*, **42**, 10084–10094.
7. Xiao, G., Liu, S., Ji, X., Johnson, W. W., Chen, J., Parsone, J. F. *et al.* (1996). First-sphere and second-sphere electrostatic effects in the active site of a class mu gluthathione transferase. *Biochemistry*, **35**, 4753–4765.
8. Stenberg, G., Board, P. G., Carlberg, I. & Mannervik, B. (1991). Effects of directed mutagenesis on conserved arginine residues in a human class alpha glutathione transferase. *Biochem. J.* **274**, 549–555.
9. Ibarra, C. A., Chowdhury, P., Petrich, J. W. & Atkins, W. M. (2003). The anomalous pK_a of Tyr-9 in glutathione S-transferase A1-1 catalyzes product release. *J. Biol. Chem.* **278**, 19257–19265.

10. Ibarra, C., Nieslanik, B. S. & Atkins, W. M. (2001). Contribution of aromatic-aromatic interactions to the anomalous p*K*(a) of tyrosine-9 and the C-terminal dynamics of glutathione S-transferase A1-1. *Biochemistry*, **40**, 10614–10624.
11. Bjornestedt, R., Stenberg, G., Widersten, M., Board, P. G., Sinning, I., Jones, T. A. & Mannervik, B. (1995). Functional significance of arginine 15 in the active site of human class alpha glutathione transferase A1-1. *J. Mol. Biol.* **247**, 765–773.
12. Stevens, J. M., Armstrong, R. N. & Dirr, H. W. (2000). Electrostatic interactions affecting the active site of class sigma glutathione S-transferase. *Biochem. J.* **347**, 193–197.
13. Dietze, E. C., Wang, R. W., Lu, A. Y. & Atkins, W. M. (1996). Ligand effects on the fluorescence properties of tyrosine-9 in alpha 1-1 glutathione S-transferase. *Biochemistry*, **35**, 6745–6753.
14. Kong, K., Takasu, K., Inoue, H. & Takahashi, K. (1992). Tyrosine-7 in human class pi glutathione S-transferase is important for lowering the pK_a of the thiol group of glutathione in the enzyme-glutathione complex. *Biochem. Biophys. Res. Commun.* **184**, 194–197.
15. Liu, S., Zhang, P., Ji, X., Johnson, W. W., Gilliland, G. L. & Armstrong, R. N. (1992). Contribution of tyrosine 6 to the catalytic mechanism of isoenzyme 3-3 of glutathione S-transferase. *J. Biol. Chem.* **267**, 4296–4299.
16. Pettersson, P. L. & Mannervik, B. (2001). The role of glutathione in the isomerization of delta 5-androstene-3,17-dione catalyzed by human glutathione transferase A1-1. *J. Biol. Chem.* **276**, 11698–11704.
17. Johansson, A. S. & Mannervik, B. (2002). Active-site residues governing high steroid isomerase activity in human glutathione transferase A3-3. *J. Biol. Chem.* **277**, 16648–16654.
18. Nyquist, R. M., Heitbrink, D., Bolwien, C., Gennis, R. B. & Heberle, J. (2003). Direct observation of protonation reactions during the catalytic cycle of cytochrome c oxidase. *Proc. Natl Acad. Sci. USA*, **22**, 8715–8720.
19. Frank, R. A., Titman, C. M., Pratap, J. V., Luisi, B. F. & Perham, R. N. (2004). A molecular switch and proton wire synchronize the active sites in thiamine enzymes. *Science*, **306**, 872–876.
20. Ortiz-Salmerón, E., Nuccetelli, M., Oakley, A. J., Parker, M. W., Lo Bello, M. & García-Fuentes, L. (2003). Thermodynamic description of the effect of the mutation Y49F on human glutathione transferase P1-1 in binding with glutathione and the inhibitor S-hexylglutathione. *J. Biol. Chem.* **278**, 46938–46948.
21. Stevens, J. M., Armstrong, R. N., Hornby, J. A. & Dirr, H. W. (1998). Class sigma glutathione transferase unfolds via a dimeric and a monomeric intermediate: impact of subunit interface on conformational stability in the superfamily. *Biochemistry*, **37**, 15534–15541.
22. Ricci, G., Caccuri, A. M., Lo Bello, M., Rosato, N., Mei, G., Nicotra, M. *et al.* (1996). Structural flexibility modulates the activity of human glutathione transferase P1-1. Role of helix 2 flexibility in the catalytic mechanism. *J. Biol. Chem.* **271**, 16187–16192.
23. Chern, M. K., Wu, T. C., Hsieh, C. H., Chou, C. C., Liu, L. F., Kuan, I. C. *et al.* (2000). Tyr115, Gln165 and Trp209 contribute to the 1 (2000)2-epoxy-3-(*p*-nitrophenoxy)propane-conjugating activity of glutathione *S*-transferase cGSTM1-1. *J. Mol. Biol.* **300**, 1257–1269.
24. Nilsson, L. O., Edalat, M., Pettersson, P. L. & Mannervik, B. (2002). Aromatic residues in the C-terminal region of glutathione transferase A1-1 influence the rate-determining steps in the catalytic mechanism. *Biochim. Biophys. Acta*, **1598**, 199–205.
25. Wongsantichon, J. & Ketterman, A. J. (2005). An intersubunit lock-and-key 'clasp' motif in the interface of Delta class glutathione transferase. *Biochem. J.* **394**, 135–144.
26. Otwinowski, Z. & Minor, W. (1997). Processing of X-ray diffraction data collected in oscillation mode. *Methods Enzymol.* **276**, 307–326.
27. Navaza, J. (1994). AMoRe: An automated package for molecular replacement. *Acta Crystallog. sect. A*, **50**, 157–163.
28. Collaborative Computational Project, Number 4. (1994). The CCP4 suite: programs for protein crystallography. *Acta Crystallog. sect. D*, **50**, 760–763.
29. Murshudov, G., Vagin, A. & Dodson, E. (1997). Refinement of macromolecular structures by the maximum likelihood method. *Acta Crystallog. sect. D*, **53**, 240–255.
30. McRee, D. E. (1999). XtalView/Xfit- a versatile program for manipulating atomic coordinates and electron density. *J. Struct. Biol.* **125**, 156–165.
31. Laskowski, R. A., MacArthur, M. W., Moss, D. S. & Thornton, J. (1993). M. PROCHECK: a program to check the stereochemical quality of protein structures. *J. Appl. Crystallog.* **26**, 283–291.
32. Emsley, P. & Cowtan, K. (2004). Coot: model-building tools for molecular graphics. *Acta Crystallog. sect. D*, **60**, 2126–2132.
33. Liang, J., Edelsbrunner, H. & Woodward, C. (1998). Anatomy of protein pockets and cavities: measurement of binding site geometry and implications for ligand design. *Protein Sci.* **7**, 1884–1897.
34. Kolm, R. H., Sroga, G. E. & Mannervik, B. (1992). Participation of the phenolic hydroxyl group of Tyr-8 in the catalytic mechanism of human glutathione transferase P1-1. *Biochem. J.* **285**, 537–540.

Edited by R. Huber

(Received 13 March 2006; received in revised form 10 May 2006; accepted 16 May 2006)
Available online 2 June 2006